Adaptive Mitigation Control for Wideband Oscillations of Offshore Wind Farms With MMC-HVDC System

Yiming Rao, Jing Lyu, *Senior Member*, *IEEE*, Yifan Wang, and Xu Cai

***Abstract*—With offshore becoming the main battlefield of wind power generation, modular multilevel converter-based high-voltage DC (MMC-HVDC) transmission technology has become an ideal solution for offshore wind power integration and received rapid development. However, wideband oscillation events have seriously threatened stable operation of power systems. By far, existing oscillation mitigation methods are usually designed for specific oscillation cases and are not capable of mitigating wideband oscillations. In order to mitigate various oscillations adaptively, this article proposes an adaptive wideband oscillation mitigation control for MMC-HVDC system connected to offshore wind farms. Analytical wideband impedance models of the wind farm side MMC (WFMMC) and offshore wind farm composed of permanent-magnetic synchronous generator-based wind turbine generators (PMSG-WTGs) are derived, respectively, which are verified by measured impedances from time-domain simulations. Then, a wideband oscillation mechanism is revealed by impedance-frequency characteristics. On this basis, an adaptive wideband oscillation mitigation control is proposed, and its working principle as well as implementation process are elaborated. Case studies of a sub-/super-synchronous oscillation (SSO) event and a high-frequency oscillation (HFO) event of an offshore wind farm with MMC-HVDC system are carried out to verify effectiveness of the proposed adaptive wideband oscillation mitigation control.**

***Index Terms*—Adaptive mitigation control, MMC-HVDC, offshore wind farm, wideband oscillation.**

I. Introduction

OFFSHORE has become the main battlefield of wind power generation due to its vast space resources and huge wind energy reserves. Among many schemes for offshore wind farm integration, modular multilevel converter-based high-voltage DC (MMC-HVDC) transmission technology has become the mainstream scheme gradually [1], [2]. Many countries in the world have carried out engineering practice of offshore wind farm with MMC-HVDC system [3], [4].

However, with rapid growth of engineering projects of offshore wind farms with MMC-HVDC system, wideband oscillation events occurred frequently in practical projects and seriously threatened stable operation of power systems [5]–[7]. These oscillations have brought a series of serious consequences. Therefore, a wideband oscillation mitigation strategy is urgently needed.

According to oscillation frequency, wideband oscillations can be classified into two types: sub-/super-synchronous oscillation (SSO, 3 to 100 Hz) and high-frequency oscillation (HFO, above 100 Hz). In existing research, oscillation mitigation methods are usually designed for specific oscillation cases, in other words, can only mitigate specific SSO or HFO.

There are three types of existing SSO mitigation methods: active damping control [8]–[11], controller parameter optimization [12], [13], and using extra equipment [14]–[17]. A virtual arm resistance control scheme for SSO mitigation was proposed in [8], but it couldn't ensure adequate damping for HFOs. A supplementary sub-synchronous damping control (SSDC) scheme was investigated in [9], in which the parameters of SSDC were carefully designed to mitigate SSO. Filter-based active damping control schemes were proposed in [10] and [11], in which bandpass filters were designed with fixed parameters according to prior torsional mode analysis, to mitigate SSOs that lie on the vicinity of known torsional modes. Controller parameters were optimized in [12] and [13] to enhance AC-side and DC-side stability of MMC-HVDC systems, respectively, but only the frequency range of SSO was considered. Extra equipment such as synchronous condenser [14], static var compensator [15], static synchronous compensator [16] and shunt voltage-source converter [17] were designed to mitigate SSOs, respectively.

Existing HFO mitigation methods are mainly based on ideas of modifying the voltage feed-forward channel [18], [19], active damping control [20]–[22] and paralleling external impedance [19]. Negative damping characteristics of high-frequency range introduced by the voltage feed-forward channel of MMC controller is one of the main reasons for HFOs, so inserting a low-pass filter into the voltage feed-forward channel [18], [19] was recognized as a simple and effective HFO mitigation method. Most active damping control schemes for HFOs were implemented by feedbacking high-

Manuscript received September 1, 2021; revised February 24, 2022; accepted April 1, 2022. Date of online publication September 8, 2023; date of current version October 8, 2023. This work was supported in part by the National Natural Science Foundation of China (51907125) and in part by the China Three Gorges Corporation (202103026).

Y. M. Rao, J. Lyu (corresponding author, email: lvjing@sjtu.edu.cn; ORCID: https://orcid.org/0000-0002-1817-7926) and X. Cai are with the Key Laboratory of Control of Power Transmission and Conversion, Ministry of Education, Shanghai Jiao Tong University, Shanghai 200240, China.

Y. F. Wang is with Science and Technology Research Institute, China Three Gorges Corporation, Beijing 101199, China.

DOI: 10.17775/CSEEJPES.2021.06530

frequency oscillation signals to the control system through high-pass filters. The harm of control delay was eliminated by a high-pass filter-based damping control in [20], so HFO risk was reduced. High-frequency damping was increased in [21] by adding additional signals processed by high-pass filters to modulation voltage signals. In [22], high-pass filters with adequate cut-off frequencies were adopted in control systems of wind power converters and wind farm side MMC (WFMMC) to implement active damping control. A third-order bandpass filter was adopted in MMC controller to increase the stability of two potentially risky HFO modes in [23]. Besides, an HFO mitigation method based on paralleling external impedance was investigated in [19], in which external impedance was provided by passive devices or small-scale converters. It is obvious the above low-/high-/band-pass filter-based methods are ineffective for SSO mitigation, and the method of paralleling external impedance brings extra cost and power loss to the project.

The aforementioned mitigation methods focus on oscillations in a specific frequency range, design control schemes or set fixed parameters according to prior mechanism analysis. Therefore, they can only mitigate oscillations of the corresponding frequency range. However, oscillations at various frequencies (from tens of hertz to thousands of hertz) may occur in a system of offshore wind farms with MMC-HVDC. Existing methods cannot effectively mitigate oscillations in such a wide frequency range, that is, cannot achieve the goal of wideband oscillation mitigation.

In order to mitigate various oscillations adaptively, this article proposes adaptive wideband oscillation mitigation control for systems of offshore wind farm with MMC-HVDC. Innovations and contributions of this article are as follows:

1) An adaptive mitigation control which is applicable to both SSOs and HFOs (i.e., wideband oscillations) in the system of offshore wind farms with MMC-HVDC is proposed, to break through limitations of existing methods which are merely suitable for SSOs or HFOs.

2) The working mode of online monitor and adaptive mitigation of wideband oscillations is studied, in which parameters of virtual resistor control loop are set adaptively based on online oscillation monitor results, so wideband oscillations with various frequencies can be mitigated and no prior mechanism analysis is required.

The remaining part is arranged as below. Section II describes structure and control of the system under study. Section III gives impedance modeling results of wind farm and WFMMC and reveals wideband oscillation mechanism. The basic principle, key function modules and implementation process of the adaptive mitigation control for wideband oscillations are elaborated in Section IV. Section V shows case study results to validate effectiveness of adaptive mitigation control. Section VI presents the conclusion.

II. System Introduction

A. System Structure

Configuration of an offshore wind farm with an MMC-HVDC system is presented in Fig. 1. The wind farm is composed of permanent-magnetic synchronous generator-based

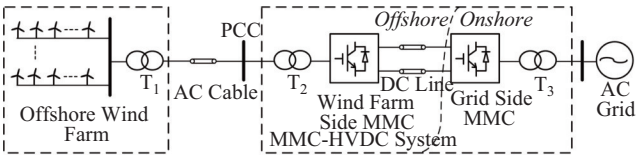

Fig. 1. Configuration of an offshore wind farm with an MMC-HVDC system.

wind turbine generators (PMSG-WTGs). The WFMMC station is offshore while the grid side MMC station is onshore. T_1, T_2 and T_3 are the wind farm step-up transformer and HVDC converter transformers, respectively. PCC is the point of common coupling.

B. System Control

1) Control of PMSG-WTG

Grid-side subsystem dynamics of PMSG-WTG can be decoupled with machine-side subsystem dynamics due to the large DC-bus capacitor, so grid-side subsystem dynamics are hardly affected by machine-side subsystem dynamics [24]. Therefore, PMSG-WTG integration characteristics can be simplified as that of a grid-side converter with a DC constant power source. Fig. 2 presents the main circuit and control of grid-side converter of PMSG-WTG. The control objective of the grid-side converter is to stabilize DC-bus voltage $U_{\rm dc}$, and in the meantime adjust output reactive power of the PMSG-WTG. Controllers of outer and inner loops, as well as the phase-locked loop (PLL) are all proportional-integral regulators.

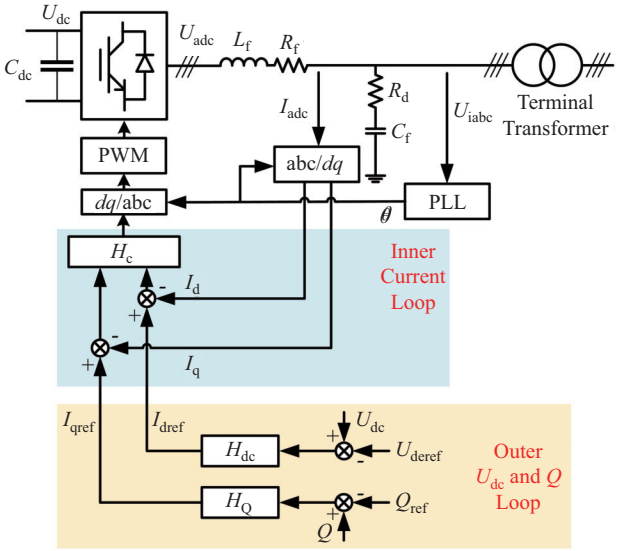

Fig. 2. Main circuit and control of the grid-side converter of PMSG-WTG.

2) Control of Wind Farm Side MMC

Figure 3 presents the control structure of WFMMC. The control objective of the WFMMC is to provide stable AC voltage of PCC for wind power integration, so its control system mainly consists outer AC voltage loop and inner current loop. In addition, a circulating current suppression controller (CCSC) is adopted to suppress internal circulating current. Controllers of outer and inner loops, as well as the

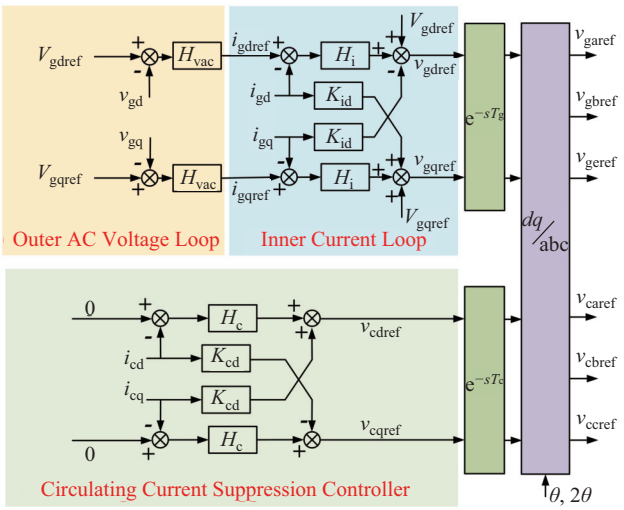

Fig. 3. Control of WFMMC.

CCSC are all proportional-integral regulators. Control delay is considered in this study.

III. System Modeling and Wideband Oscillation Mechanism Analysis

A. Impedance Models of the Studied System

Wideband impedance models of wind farm and WFMMC are derived analytically in this work. Since impedance models of the PMSG-WTG and MMC have been elaborated in our previous work [24], [25], modeling processes are not presented in this article.

Simulation models of the PMSG-WTG and WFMMC are built in Simulink to validate derived wideband impedance models. Tables I and II show electrical parameters of PMSG-WTG and WFMMC, respectively.

TABLE I
Main Electrical Parameters of PMSG-WTG

Parameters		Value
PMSG	Rated capacity	4 MW
	Pole pairs	32
	Flux linkage	8.4 Wb
	Stator resistance	46.1 mΩ
	Mutual inductance	17.2 mH
	Rated rpm	120
Grid side converter	Rated DC-bus voltage	1120 V
	Capacitance of DC-bus	32.64 mF
	Rated AC-side voltage	690 V
	Filter parameters (L_f, R_f, C_f, R_d)	(0.03 mH, 0. 471 mΩ, 0.9469 mF, 59.3 mΩ)

TABLE II
Main Electrical Parameters of WFMMC

Parameters	Value
Rated power	1100 MW
Rated AC-side voltage	416 kV
Rated DC-bus voltage	± 400 kV
Arm inductance	133 mH
Submodule number per arm	400
Capacitance of submodule	11 mF

Figures 4 and 5 exhibit comparisons of analytical impedances from impedance models and measured impedances from simulations of PMSG-WTG and WFMMC, respectively. It is clear analytical impedances of the PMSG-WTG and WFMMC have good consistency with measured impedances within the full frequency range. Therefore, derived wideband impedance models are accurate.

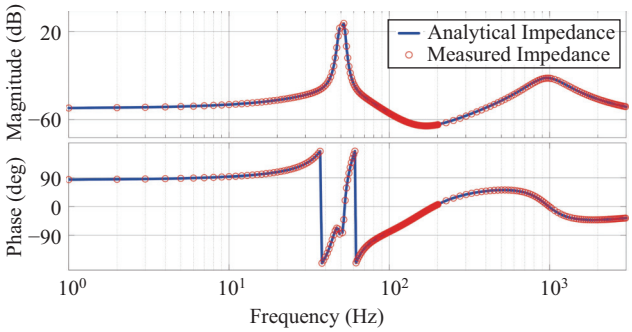

Fig. 4. PMSG-WTG wideband impedance model validation.

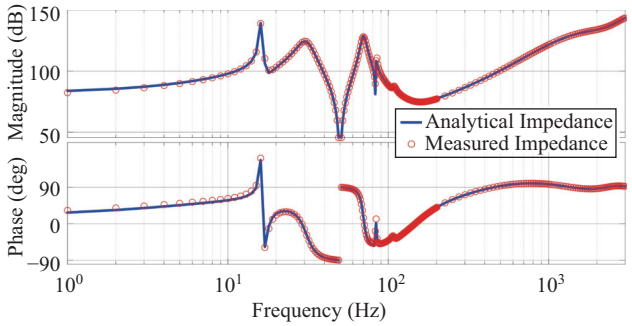

Fig. 5. WFMMC wideband impedance model validation.

B. Wideband Oscillation Mechanism Analysis

Based on derived impedance models, two oscillatory cases, an SSO event (Case 1) and an HFO event (Case 2) of an actual offshore wind farm with an MMC-HVDC system are carried out to reveal wideband oscillation mechanism by impedance-frequency characteristics. The offshore wind farm is comprised of 275 PMSG-WTGs. System parameters are the same as Tables I and II.

1) Mechanism of SSO

As shown in Fig. 6, impedance magnitude of the wind farm shows a downward trend in frequency range below 100 Hz as wind farm output power increases. Magnitude-frequency characteristics of WFMMC impedance contain resonance peaks at both ends of the fundamental frequency (50 Hz). Based on analysis of WFMMC impedance characteristics, it is found such resonance peaks are introduced by its current control and internal dynamics. With wind farm output power increases, the magnitude-frequency curve of the wind farm impedance is likely to intersect with resonance peaks of WFMMC impedance, and when the corresponding phase difference is close to or exceeds 180°, stability margin is inadequate or negative, the interconnected system will oscillate at the intersection frequency. That's the main mechanism of

SSOs. In Case 1, intersection frequency and stability margin are 65 Hz and −0.48°, respectively, as shown in Fig. 6.

2) Mechanism of HFO

As illustrated in Fig. 7, the wind farm shows capacitive characteristics in most of the high-frequency ranges. On the contrary, phase of WFMMC impedance is positive and exceeds 90° in some frequency ranges, indicating WFMMC presents as an inductor along with a negative resistor in some frequency ranges. Besides, negative resistor characteristics are enhanced as control delay of the WFMMC increases, which are likely to cause negative stability margin of the interconnected system. Therefore, control delay of WFMMC is the mechanism of HFOs. In Case 2, the HFO frequency is 685 Hz.

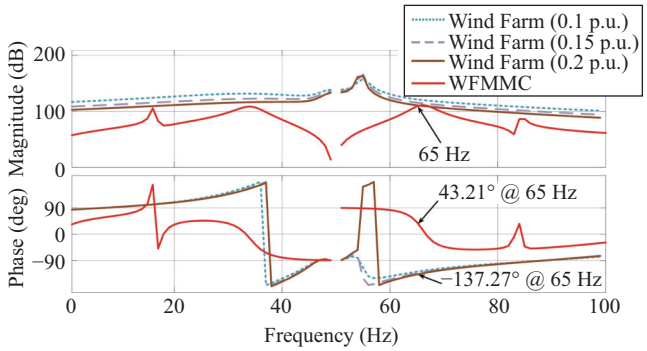

Fig. 6. Impedance-based SSO mechanism analysis (Case 1).

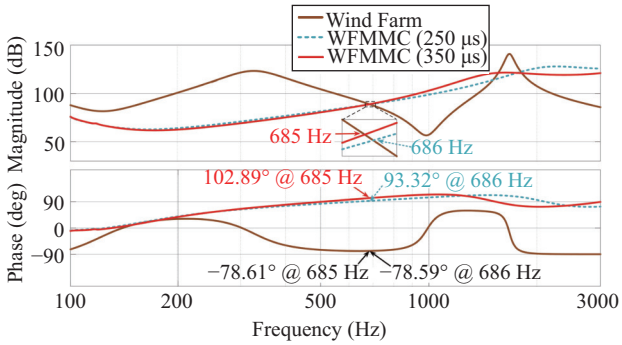

Fig. 7. Impedance-based HFO mechanism analysis (Case 2).

IV. Adaptive Mitigation Control for Wideband Oscillations

A. Basic Principle of Adaptive Mitigation Control

Adaptive mitigation control can be configured in controllers of PMSG-WTG or WFMMC. Fig. 8 shows the control structure of adaptive mitigation control applied in WFMMC controller. The adaptive mitigation control mainly consists of four parts: virtual resistor control loop (VRCL), online oscillation monitor, adaptive parameter setting and activation. The online oscillation monitor recognizes the real-time dominant oscillation frequency (DOF) f_O and content of dominant oscillation component (CDOC) C_O of PCC current through the sliding rectangular-windowed fast Fourier transform (FFT). C_O is the dominant oscillation component content relative to fundamental current component. The activation module determines whether to enable VRCL by examining whether the content of dominant oscillation component has exceeded the pre-set threshold C_S. Once C_O exceeds C_S, f_O is transmitted to the adaptive parameter setting module to set parameters for the VRCL. In the meantime, the activation module outputs a triggering signal S_T to activate VRCL which can well mitigate monitored oscillation.

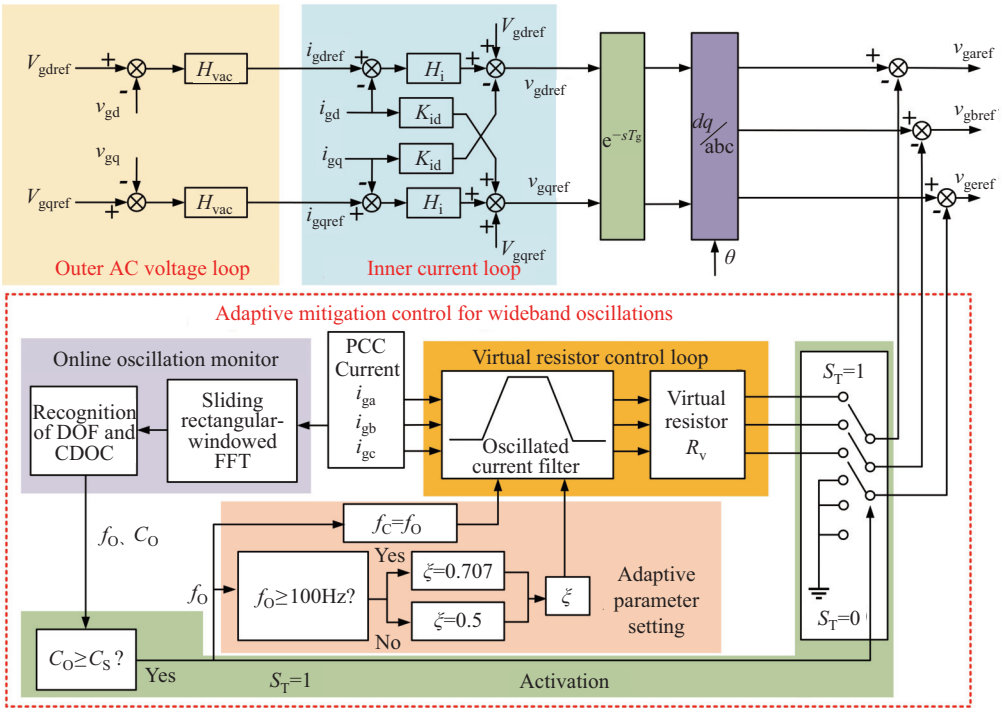

Fig. 8. Adaptive mitigation control applied in WFMMC.

Parameters of the VRCL are adaptively adjusted according to online monitored oscillation frequency, so the proposed adaptive mitigation control can mitigate oscillations at various frequencies.

The four key function modules of the proposed adaptive mitigation control are introduced in detail as follows, respectively.

B. Key Function Modules of Adaptive Mitigation Control

1) Virtual Resistor Control Loop

As presented in Fig. 8, VRCL consists of an oscillated current filter and a virtual resistor R_{V}. The oscillated current filter is essentially a bandpass filter which only allows input components near its center frequency f_{C} to pass through. Transfer function of the bandpass filter can be expressed as

$$G_{\mathrm{bp}}(s)=\frac{2\xi\omega_{\mathrm{C}}s}{s^2+2\xi\omega_{\mathrm{C}}s+\omega_{\mathrm{C}}^2} \tag{1}$$

in which damping ratio ξ and center angular frequency ω_{C} together determine bandwidth f_{BW} of the bandpass filter, that is.

$$f_{\mathrm{BW}}=2\xi f_{\mathrm{C}}=2\xi\frac{\omega_{\mathrm{C}}}{2\pi} \tag{2}$$

In the proposed adaptive mitigation control, the oscillated current filter is used to filter out the oscillated current component of PCC current. Since supplementary control signals of VRCL are superposed to modulation voltage signals of WFMMC, filtered oscillated current signals should be amplified by a virtual resistor R_{V}. Essentially, VRCL superimposes a voltage component whose phase is opposite to oscillation voltage to the original modulation signal of WFMMC. R_{V} determines magnitude of the superimposed voltage component, and its setting method will be discussed in detail later. Therefore, VRCL plays a role in blocking propagation of oscillation components, so corresponding oscillation can be mitigated.

2) Online Oscillation Monitor

Figure 9 shows the working process of online oscillation monitor. PCC current signal is sampled by a rectangular window to acquire real-time current data. Sampling rate is f_{S} and length of the rectangular window is N/f_{S}. To ensure real-time characteristics of current data, the rectangular window should slide every other period of time, and time step is Δt. With sampled real-time current data, DOF f_{O} and CDOC C_{O}

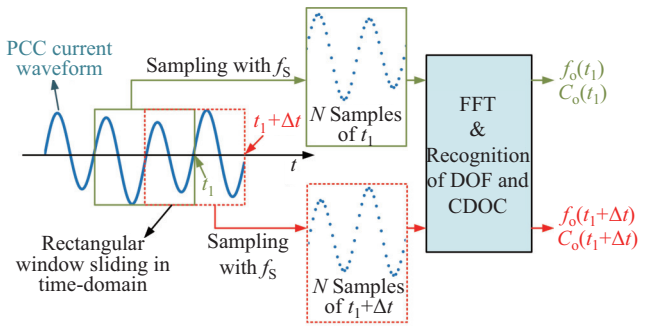

Fig. 9. Working process of online oscillation monitor.

can be obtained by applying FFT to current data. If there are multiple oscillation components at the same time, the one with highest amplitude is considered as the dominant oscillation component.

3) Adaptive Parameter Setting

There are three parameters that need to set for the VRCL, R_{V}, f_{C} and ξ.

Virtual resistor R_{V} is used to amplify filtered oscillated current signals, and amplified signals are superposed to the modulation voltage signals of WFMMC. Therefore, the order of magnitude of R_{V} is the same as the ratio between the rated phase voltage and current of WFMMC, that is

$$R_{\mathrm{V}}\approx\frac{v_{\mathrm{gN}}}{i_{\mathrm{gN}}} \tag{3}$$

After determining the order of magnitude of R_{V} using (3), fine-tuning can be performed to achieve better oscillation mitigation effect.

In order to filter out the dominant oscillated component of PCC current, DOF f_{O} needs to be within the passband of the bandpass filter. Therefore, as shown in Fig. 8, DOF f_{O} is used as the bandpass filter center frequency f_{C}.

Damping ratio can be set according to oscillation types. According to our previous research, oscillation frequency of SSO is relatively onefold. In other words, compared with the dominant SSO component, amplitudes of other oscillation components in the vicinity of the dominant SSO component are negligible. Therefore, in an SSO event, it can be considered the oscillated PCC current only contains oscillated components of the dominant oscillation frequency and its mirror frequency. However, there are many oscillation components around the dominant HFO component in frequency-domain, which cannot be ignored due to their large amplitudes. In order to select oscillation components of AC current, bandwidth of the bandpass filter should be designed properly according to spectrum characteristics of different oscillations. When an SSO occurs, the passband of the bandpass filter is supposed to be a bit narrower to accurately select the SSO component. When an HFO occurs, the bandwidth should be wider to make the bandpass filter select the dominant HFO component while taking oscillation components in the vicinity of dominant HFO component into account.

According to (2), when monitored oscillation frequency is lower than 100 Hz, indicating an SSO occurred, damping ratio is supposed to be set as a smaller value, while damping ratio for HFOs can be larger to make the bandwidth wider.

In addition, damping ratio should be designed to ensure adequate damping of the interconnected system. With the derived WFMMC impedance model, wideband impedance curves of WFMMC with VRCL of different damping ratios can be obtained.

In Case 1, impedance curves of WFMMC with VRCL of different damping ratios are shown in Fig. 10. For clarity, black dashed arrows are used to indicate the trend of WFMMC impedance curves as damping ratio increases. It is clear as damping ratio increases, WFMMC impedance magnitude shows a downward trend in the frequency range below 50 Hz, especially, impedance magnitude around the resonance peak

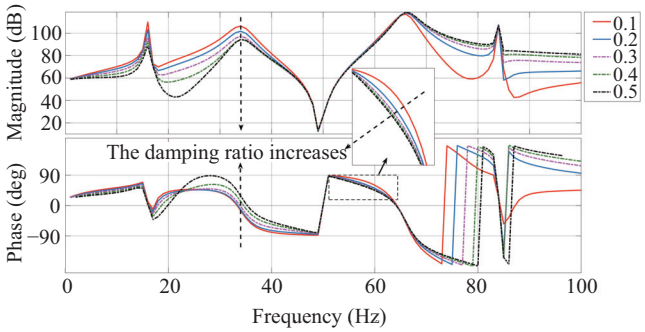

Fig. 10. Impedance curves of WFMMC with VRCL of different damping ratios (Case 1, $f_C = 65$ Hz).

is reduced and the corresponding phase is increased. In the frequency range of 50 to 100 Hz, the resonance peak remains almost unchanged, but the impedance phase at the frequency below resonance frequency is reduced with damping ratio increase. Combined with SSO mechanism analysis, it can be found the larger the damping ratio, the more damping is added to the system.

In Case 2, impedance-frequency characteristics of WFMMC with VRCL of different damping ratios are shown in Fig. 11.

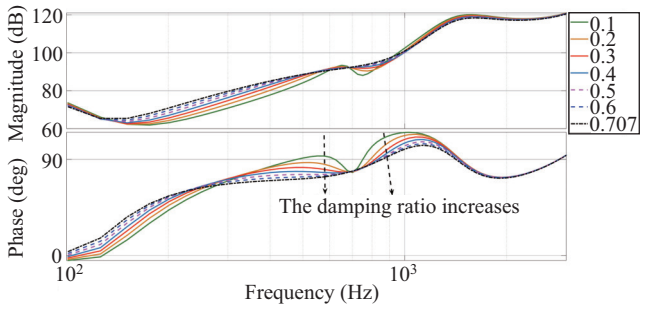

Fig. 11. Impedance curves of WFMMC with VRCL of different damping ratios (Case 2, $f_C = 685$ Hz).

As illustrated in Fig. 11, with damping ratio increase, the WFMMC impedance phase in the frequency range of HFO risk is decreased as indicated by the black dashed arrows, i.e., the negative damping of WFMMC is weakened. Therefore, VRCL with a larger damping ratio performs better in mitigation of HFOs.

To summarize the above analysis, to ensure adequate damping of the interconnected system, larger damping ratios are preferred, irrespective of SSOs or HFOs.

Comprehensively considering bandpass filter bandwidth and impacts of damping ratio on WFMMC impedance characteristics, damping ratio for SSOs cannot be set too large or too small, to make the bandpass filter accurately select the SSO component and ensure adequate damping when the VRCL is activated. By trade-off, the damping ratio for SSOs can be selected as 0.5.

Damping ratio of a bandpass filter is typically a value between 0 and 1. Considering characteristics of SSO and HFO, a damping ratio larger than the one selected for SSOs is supposed to be selected for HFOs. Therefore, the damping ratio for HFOs can be selected as 0.707 which is the optimal damping ratio for second order systems. In the meantime, the damping ratio of 0.707 can ensure adequate damping of the system.

Damping ratio of bandpass filter is not unique. In practical engineering, damping ratio can be selected based on the actual situation. For instance, a larger damping ratio is preferred for a system with weak damping.

4) Activation of Virtual Resistor Control Loop

Threshold C_S is a percentage indicating that the oscillation component reaches a certain proportion of the fundamental component. To ensure sensitivity and reliability of the proposed adaptive mitigation control, C_S should be designed properly. Considering sensitivity, VRCL should be sensitive enough to be enabled immediately when an oscillation occurs, so C_S cannot be set too large. Considering reliability, preventing the VRCL from wrong actions due to noise interference, C_S cannot be set too small.

The technical rule of China for wind farm integration requires the total harmonic distortion (THD) of wind farm current should not exceed 5%. That is to say, when THD of the wind farm output current is lower than 5%, the system can be considered to be operating in a normal state. Therefore, C_S can be determined as 5%.

Threshold C_S is not unique, and it can be adjusted appropriately based on the actual situation and relevant regulations of the region where the project is located.

When the content of dominant oscillation component C_O exceeds threshold C_S, the activation module outputs a triggering signal S_T to activate the VRCL whose parameters have been set adaptively according to online oscillation monitor results.

V. Case Study

A simulation model of a practical offshore wind farm with an MMC-HVDC system has been built in Simulink. Simulations of Case 1 and Case 2 are conducted to validate efficacy of the proposed adaptive wideband oscillation mitigation control strategy.

A. Case 1: An SSO Event

Frequency-domain analysis results of Case 1 are shown in Fig. 12, in which wind farm outputs active power of 0.2 p.u.

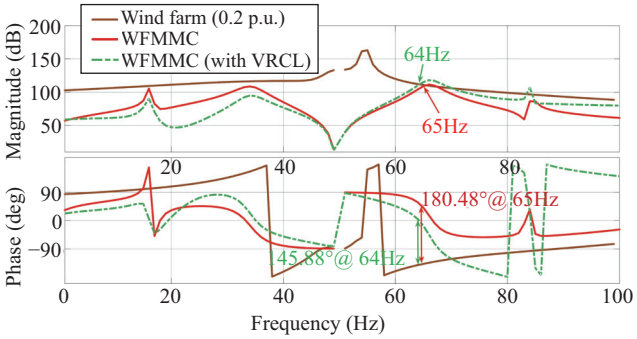

Fig. 12. Frequency-domain analysis of Case 1.

As indicted by the red arrow, the system without VRCL faces an SSO risk of 65 Hz.

The proposed adaptive mitigation control monitors the oscillation component online, then sets parameters for the VRCL according to the monitor results and attaches the VRCL to the WFMMC controller. As indicated by the green dashed line in Fig. 12, stability margin has been improved to a positive value of 34.12° by the attached VRCL, meaning the interconnected system with the proposed adaptive mitigation control is stable.

In the simulation of Case 1, initial wind farm output level is set to 0.1 p.u., then it is increased to 0.2 p.u. at 2 s. Fig. 13 exhibits simulation results. It shows PCC current increases gradually after the wind farm output level is increased to 0.2 p.u. at 2 s, then the waveform becomes distorted. FFT analysis results of the current waveform indicate the oscillated frequencies are 65 Hz and 35 Hz, in which 65 Hz is the dominant oscillation frequency. The oscillation component of 35 Hz is generated by the mirror frequency coupling [26]. The simulation results are identical to the oscillation frequency predicted in Figs. 6 and 12.

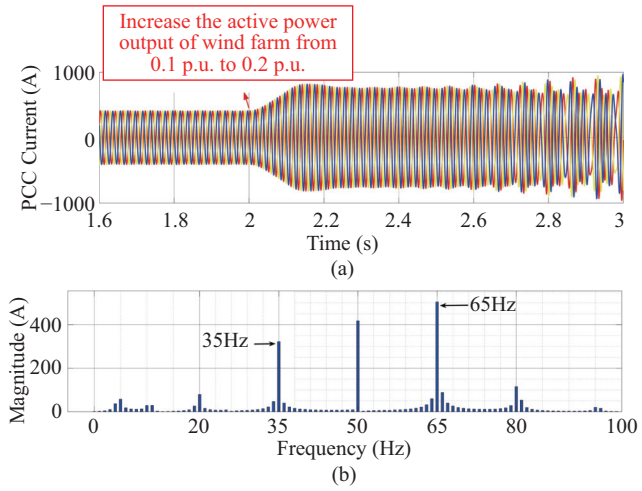

Fig. 13. Simulation results of Case 1 without adaptive mitigation control. (a) PCC current waveform. (b) FFT analysis results of the PCC current.

Then adaptive mitigation control is applied to the simulation of Case 1. Parameters of the online oscillation monitor are selected as: sampling rate $f_S = 100$ kHz, time step $\Delta t = 0.005$ s, number of samples $N = 20000$. Threshold $C_S = 5\%$.

In the same way, wind farm output level is increased to 0.2 p.u. at 2 s. Simulation results with adaptive mitigation control are exhibited in Fig. 14. It shows dominant oscillation component with frequency of 65 Hz is recognized by the online oscillation monitor at 2.255 s, and amplitude of the oscillation component is monitored continuously. Relative content of dominant oscillation component exceeds the threshold 5% at 2.45 s. According to online monitor results, the VRCL is set adaptively and put into use automatically. Then SSO is well mitigated, as illustrated by Fig. 14(a).

B. Case 2: An HFO Event

Frequency-domain analysis results of Case 2 are shown in Fig. 15. As indicted by the red arrow, the system without

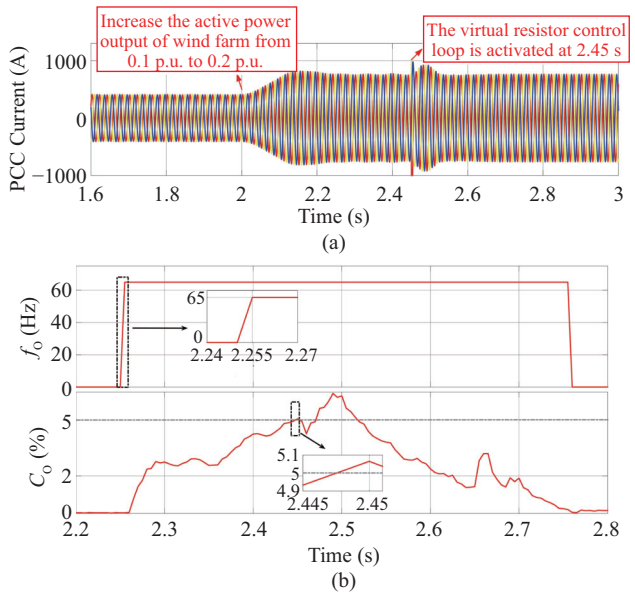

Fig. 14. Simulation results of Case 1 with adaptive mitigation control. (a) PCC current waveform. (b) Outputs of online oscillation monitor.

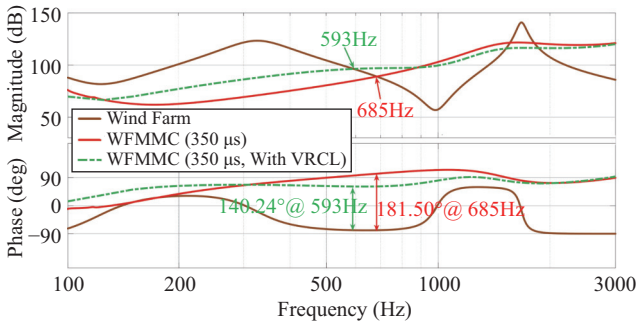

Fig. 15. Frequency-domain analysis of Case 2.

VRCL suffers from an HFO risk of 685 Hz when the WFMMC controller has a control delay of 350 μs.

Similarly, the proposed adaptive mitigation control detects the oscillation component online and attaches corresponding VRCL to the controller of WFMMC. It is observed in Fig. 15 with VRCL, negative resistor characteristics of WFMMC impedance disappear. As indicated by the green dashed line in Fig. 15, stability margin has been improved to a positive value of 39.76° by the attached VRCL, meaning the interconnected system with the proposed adaptive mitigation control is stable.

In the simulation of Case 2, initial control delay of WFMMC is set to 250 μs, then it is increased to 350 μs at 0.8 s. Fig. 16 shows simulation results. It is clear PCC current waveforms diverge gradually, and FFT analysis results show an HFO of 685 Hz is aroused in the system. Dominant oscillation frequency is identical to oscillation frequency predicted in Fig. 7 and 15.

The proposed adaptive mitigation control is then applied to simulation model of Case 2. Parameters of the online oscillation monitor and threshold are the same as Section V-A.

Control delay of WFMMC is increased to 350 μs at 0.8 s. Fig. 17 shows simulation results. It's observed the three-phase currents at PCC oscillates after control delay is increased.

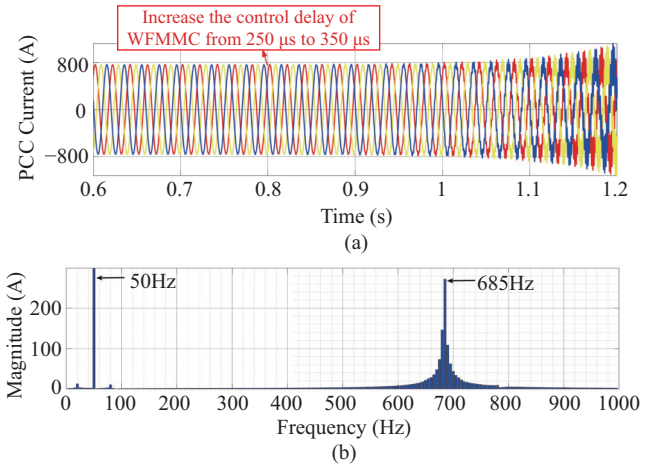

Fig. 16. Simulation results of Case 2 without adaptive mitigation control. (a) PCC current waveform. (b) FFT analysis results of the PCC current.

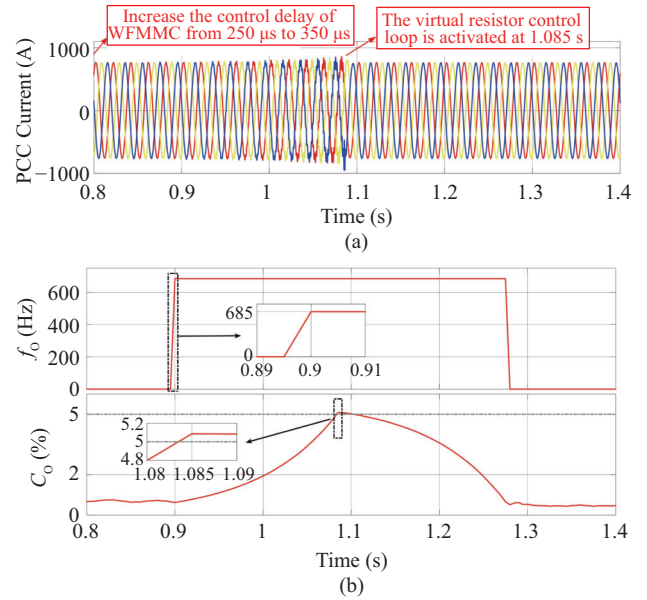

Fig. 17. Simulation results of Case 2 with adaptive mitigation control. (a) PCC current waveform. (b) Outputs of online oscillation monitor.

The online oscillation monitor recognizes dominant oscillation frequency of 685 Hz at 0.9 s, then amplitude of the oscillation component is monitored continuously. At 1.085 s, the C_O exceeds threshold 5%, then VRCL is set adaptively and activated automatically. As a result, the HFO is well mitigated.

VI. Conclusion

An adaptive mitigation control for offshore wind farms with an MMC-HVDC system was proposed in this article to mitigate various oscillations adaptively. Efficacy of the proposed adaptive mitigation control is verified by two oscillatory cases of a practical MMC-HVDC system for offshore wind farms. Conclusions can be obtained from this work:

1) The proposed adaptive mitigation control strategy is applicable to mitigate both SSOs and HFOs of the interconnected system adaptively.

2) A virtual resistor control loop can ensure adequate damping of the interconnected system by tuning its damping ratio. The larger the damping ratio, the more damping is added to the interconnected system.

3) The proposed working mode of online monitor and adaptive mitigation of wideband oscillations has good performance in the studied system.

References

[1] J. Lyu, X. Cai, and M. Molinas, "Frequency domain stability analysis of MMC-based HVdc for wind farm integration," *IEEE Journal of Emerging and Selected Topics in Power Electronics*, vol. 4, no. 1, pp. 141–151, Mar. 2016.

[2] J. Y. Li, X. H. Wang, J. Lyu, H. X. Zong, T. Xue, Z. X. Fang, and X. Cai, "Stability analysis of wind farm connected to hybrid HVDC converter," in *Proceedings 2020 IEEE 9th International Power Electronics and Motion Control Conference (IPEMC2020-ECCE Asia)*, Nanjing, China, 2020, pp. 3258–3262.

[3] K. Ji, H. Pang, J. Yang, and G. F. Tang, "DC side harmonic resonance analysis of MMC-HVDC considering wind farm integration," *IEEE Transactions on Power Delivery*, vol. 36, no. 1, pp. 254–266, Feb. 2021.

[4] K. Ji, G. F. Tang, H. Pang, and J. Yang, "Impedance modeling and analysis of MMC-HVDC for offshore wind farm integration," *IEEE Transactions on Power Delivery*, vol. 35, no. 3, pp. 1488–1501, Jun. 2020.

[5] Y. J. Yu, X. Z. Cheng, C. Zhang, and X. Q. Ji, "Oscillation mechanism and mitigation of MMC-HVDC based on bifurcation theory for wind farm integration," *IEEE Access*, vol. 8, pp. 125121–125129, Jul. 2020.

[6] Y. F. Wang, C. Y. Zhao, C. Y. Guo, and A. U. Rehman, "Dynamics and small signal stability analysis of PMSG-based wind farm with an MMC-HVDC system," *CSEE Journal of Power and Energy Systems*, vol. 6, no. 1, pp. 226–235, Mar. 2020.

[7] Y. N. Chi, B. J. Tang, J. B. Hu, X. S. Tian, H. Y. Tang, Y. Li, S. J. Sun, L. Shi, and L. Shuai, "Overview of mechanism and mitigation measures on multi-frequency oscillation caused by large-scale integration of wind power," *CSEE Journal of Power and Energy Systems*, vol. 5, no. 4, pp. 433–443, Dec. 2019.

[8] J. Lyu, X. Cai, M. Amin, and M. Molinas, "Sub-synchronous oscillation mechanism and its suppression in MMC-based HVDC connected wind farms," *IET Generation, Transmission & Distribution*, vol. 12, no. 4, pp. 1021–1029, Feb. 2018.

[9] H. K. Liu, X. R. Xie, J. B. He, T. Xu, Z. Yu, C. Wang, and C. Y. Zhang, "Subsynchronous interaction between direct-drive PMSG based wind farms and weak AC networks," *IEEE Transactions on Power Systems*, vol. 32, no. 6, pp. 4708–4720, Nov. 2017.

[10] T. Joseph, C. E. Ugalde-Loo, S. Balasubramaniam, J. Liang, and G. Li, "Experimental validation of an active wideband SSR damping scheme for series-compensated networks," *IEEE Transactions on Power Delivery*, vol. 35, no. 1, pp. 58–70, Feb. 2020.

[11] K. M. Alawasa and Y. A. R. I. Mohamed, "A simple approach to damp SSR in series-compensated systems via reshaping the output admittance of a nearby VSC-based system," *IEEE Transactions on Industrial Electronics*, vol. 62, no. 5, pp. 2673–2682, May 2015.

[12] J. Lyu, X. Cai, and M. Molinas, "Optimal design of controller parameters for improving the stability of MMC-HVDC for wind farm integration," *IEEE Journal of Emerging and Selected Topics in Power Electronics*, vol. 6, no. 1, pp. 40–53, Mar. 2018.

[13] Z. Y. Li, Z. Wang, Y. Wang, T. Y. Yin, N. Mei, B. Yue, and W. J. Lei, "Accurate impedance modeling and control strategy for improving the stability of DC system in multiterminal MMC-based DC grid," *IEEE Transactions on Power Electronics*, vol. 35, no. 10, pp. 10026–10049, Oct. 2020.

[14] Y. Z. Wang, L. Wang, and Q. R. Jiang, "Impact of synchronous condenser on sub/super-synchronous oscillations in wind farms," *IEEE Transactions on Power Delivery*, vol. 36, no. 4, pp. 2075–2084, Aug. 2021.

[15] X. S. Tian, Y. N. Chi, Y. Li, H. Y. Tang, C. Liu, and Y. Y. Su, "Coordinated damping optimization control of sub-synchronous oscillation for DFIG and SVG," *CSEE Journal of Power and Energy Systems*, vol. 7, no. 1, pp. 140–149, Jan. 2021.

[16] A. Moharana, R. K. Varma, and R. Seethapathy, "SSR alleviation by STATCOM in induction-generator-based wind farm connected to series compensated line," *IEEE Transactions on Sustainable Energy*, vol. 5, no. 3, pp. 947–957, Jul. 2014.

[17] F. Zhang, C. Q. Yin, H. Z. Li, X. R. Xie, C. Hong, H. Yuan, and Y. J. Liu, "Shunt VSC based subsynchronous damping control for DFIG-based wind farms connected to an MMC-HVDC system," in *Proceedings 2020 IEEE Region 10 Conference (TENCON)*, Osaka, Japan, Nov. 2020, pp. 1029–1033.
[18] J. H. Zhu, J. B. Hu, L. Lin, Y. F. Wang, and C. Wei, "High-frequency oscillation mechanism analysis and suppression method of VSC-HVDC," *IEEE Transactions on Power Electronics*, vol. 35, no. 9, pp. 8892–8896, Sep. 2020.
[19] C. Y. Zou, H. Rao, S. K. Xu, Y. Li, W. W. Li, J. Chen, X. B. Zhao, Y. Yang, and B. Lei, "Analysis of resonance between a VSC-HVDC converter and the AC grid," *IEEE Transactions on Power Electronics*, vol. 33, no. 12, pp. 10157–10168, Dec. 2018.
[20] B. Pang, H. Nian, and Y. Y. Xu, "Mechanism analysis and damping method for high frequency resonance between VSC-HVDC and the wind farm," *IEEE Transactions on Energy Conversion*, vol. 36, no. 2, pp. 984–994, Jun. 2021.
[21] A. W. Korai and I. Erlich, "Mitigation of harmonic instability in offshore wind farms using supplementary signals in the HVDC control," in *Proceedings 2017 IEEE Power & Energy Society General Meeting*, Chicago, IL, USA, Jul. 2017, pp. 1–5.
[22] M. Cheah-Mane, L. Sainz, E. Prieto-Araujo, and O. Gomis-Bellmunt, "Impedance-based analysis of harmonic instabilities in HVDC-connected offshore wind power plants," *International Journal of Electrical Power & Energy Systems*, vol. 106, pp. 420–431, Mar. 2019.
[23] Y. F. Li, H. Pang, M. Kong, J. J. Lu, K. Ji and G. F. Tang, "Compensation control and parameters design for high frequency resonance suppression of MMC-HVDC system," *CSEE Journal of Power and Energy Systems*, vol. 7, no. 6, pp. 1161–1175, Nov. 2021.
[24] T. Xue, J. Lyu, H. Wang, and X. Cai, "A complete impedance model of a PMSG-based wind energy conversion system and its effect on the stability analysis of MMC-HVDC connected offshore wind farms," *IEEE Transactions on Energy Conversion*, vol. 36, no. 4, pp. 3449–3461, Dec. 2021.
[25] J. Lyu, X. Zhang, X. Cai, and M. Molinas, "Harmonic state-space based small-signal impedance modeling of a modular multilevel converter with consideration of internal harmonic dynamics," *IEEE Transactions on Power Electronics*, vol. 34, no. 3, pp. 2134–2148, Mar. 2019.
[26] A. Rygg, M. Molinas, C. Zhang, and X. Cai, "A modified sequence-domain impedance definition and its equivalence to the dq-domain impedance definition for the stability analysis of AC power electronic systems," *IEEE Journal of Emerging and Selected Topics in Power Electronics*, vol. 4, no. 4, pp. 1383–1396, Dec. 2016.

Yiming Rao received the B.Eng. degree in Electrical Engineering and Automation from Shanghai Jiao Tong University, Shanghai, China, in 2021. He is currently pursuing the M.Eng. degree in Electrical Engineering at Shanghai Jiao Tong University, Shanghai, China. His current research interests include modeling of power electronic converters, wind farm integration, MMC-HVDC, and application of artificial intelligence in power electronic systems.

Jing Lyu received the B.Eng. degree in Electrical Engineering and Automation from China University of Mining and Technology, Jiangsu, China, in 2009, the M.Eng. and Ph.D. degrees from Shanghai Jiao Tong University, Shanghai, China, in 2011 and 2016, respectively, both in Electrical Engineering. He was a Postdoctoral Research Fellow with the Department of Engineering Cybernetics, Norwegian University of Science and Technology, Trondheim, Norway, from 2016 to 2017. Since 2018, he has been with the Department of Electrical Engineering, Shanghai Jiao Tong University, where he is currently a tenure-track Associate Professor. His main research interests include dynamic stability of HVDC connected renewable energy and application of artificial intelligence in power electronic systems. Dr. Lyu is recipient of the IET Premium Awards 2020.

Yifan Wang received his Ph.D. degree in Power Systems and Its Automation from NCEPU, Beijing, China, in 2020. He is currently an Electrical Engineer with the Science and Technology Research Institute, China Three Gorges Corporation, Beijing, China. His research interests include offshore wind power integration via HVDC transmission and stability of power-electronized power systems.

Xu Cai received the B.Eng. degree in Electrical Engineering from Southeast University, Nanjing, China, in 1983, the M.Eng. and Ph.D. degrees from China University of Mining and Technology, Jiangsu, China, in 1988 and 2000, respectively, both in Electrical Engineering. He was with the Department of Electrical Engineering, China University of Mining and Technology, as an Associate Professor from 1989 to 2001. He was the Vice Director of the State Energy Smart Grid R&D Center, Shanghai, China, from 2010 to 2013. He has been with Shanghai Jiao Tong University, as a Professor since 2002, where he has also been the Director of the Wind Power Research Center since 2008. His current research interests include large power electronics, wind power generation and grid integration, HVDC, large power battery storage systems, etc.